Third International Symposium on Marine Propulsors
smp'13, Launceston, Tasmania, Australia, May 2013

The Effect of a Fixed Foil on Ship Propulsion and Motions

Eirik Bøckmann[1], **Sverre Steen**[1]

[1]Department of Marine Technology, Norwegian University of Science and Technology (NTNU), Trondheim, Norway

ABSTRACT

In this paper, we study a ship employing a fixed horizontal foil for motion reduction and thrust generation in waves. Although simple, such a foil may substantially reduce the ship motions and resistance in waves. Model tests of a 1:16 scale model of a 90 m long offshore vessel with a fixed foil of 29 m span in the bow were performed. For a ship speed of 12 knots, the fixed foil resulted in a resistance reduction of 60% in regular head sea waves with height 3.7 m and period 8.6 s. For the same wave and ship speed, the vessel's heave and pitch motions were reduced by 42% and 45%, respectively. The effect of the foil was implemented in the MARINTEK Vessel Simulator (VeSim), which solves the equations of motion for a ship in the time domain. Simulations are compared with the model tests. The ship resistance was underpredicted in the simulations for most wave periods, but this was found to be due to the foil not being entirely fixed in the model tests. The effects of longitudinal position of the foil and wave direction on the foil thrust are also studied theoretically.

Keywords

Fixed foil, wave propulsion, motion reduction.

1 INTRODUCTION

The motivation for this work is an interest in utilizing wave energy for propulsion of ships. It is known that whalers throughout history cut off the flukes of the whales they had killed, as it was observed that a dead whale propelled itself forward at a speed of about 1 knot due to the action of the sea (Bose & Lien, 1990). The propulsion of the dead whale is caused by inflow at an angle of attack to the fluke, producing a net forward force. The same principle can be applied for a ship using foils instead of flukes. In his 1858 patent, Vrooman (1858) describes a boat employing flexible fins along the hull in order to gain propulsive thrust from the waves. 40 years later, Linden received world-wide attention for his wave-powered boat (The New York Times, 1898; Ashburton Guardian, 1897; Burnett, 1979). As flexible fins, Linden's boat used two underwater steel plates, one at the bow and one at the stern.

A milestone in the development of wave-powered boats was Einar Jakobsen's introduction of the spring-loaded foil (Jakobsen, 1981). The spring-loaded foil is free to pivot about a point located in front of the center of pressure, so that it will reduce its angle of attack in an incoming flow. A spring ensures that the maximum angle of attack is not reduced to zero, but instead to a value that is – ideally – just below the stalling limit. By tuning the spring stiffness for the wave conditions, a large thrust can be obtained.

An actively controlled pitching foil has also been proposed (Naito & Isshiki, 2005; Politis & Politis, 2012). The actively controlled foil is automatically controlled to avoid stall, and should thus in theory be a better solution than the spring-loaded foil, as there is no need to constantly tune the spring stiffness in an irregular sea.

One of the main intentions of the work behind this paper has been to develop a tool for simulating a ship with horizontal foils for propulsion and motion reduction in waves. In order to include the non-harmonically varying foil forces of drag and lift due to nonlinear drag and lift coefficient curves, the simulations must be done in the time domain. We have chosen to implement foils in the MARINTEK Vessel Simulator (VeSim), which is a time-domain simulation tool. VeSim is relatively user friendly, and can simulate changing wave conditions in a single simulation run, which is convenient. In addition, VeSim contains models for the propeller and engine, so that actual fuel savings can be calculated, and not only resistance reduction. In our implementation of fixed foils in VeSim, the effect of dynamic stall is accounted for by implementing the Beddoes-Leishman dynamic stall model (Leishman & Beddoes, 1989) with some minor simplifications. This dynamic stall model is only strictly valid for two-dimensional foils, but we assume that by summing up sectional forces on a high aspect ratio foil, the model error is small.

2 SHIP RESPONSE COMPUTATION IN VESIM

2.1 Reference frames

Before we study how the six degrees of freedom motions of a ship can be calculated, let us first look at the coordinate systems, or reference frames, involved. The following definitions are taken from Fossen (2011) and Hoff (2007).

The *North-East-Down* (NED) inertial coordinate system $\{n\} = (x_n, y_n, z_n)$ with origin o_n is defined relative to the Earth's reference ellipsoid (NIMA, 1997). The $x_n y_n$-plane is usually defined as the tangent plane on the surface of the Earth moving with the craft. The x-axis points true *north*, the y-axis points towards *east*, whereas the z-axis points *downwards* normal to the surface of the Earth. The $\{n\}$-frame position $\mathbf{p}^n = [n, e, d]^T$ and Euler angles

$\boldsymbol{\Theta} = [\phi, \theta, \psi]^T$ are defined in terms of the vector

$$\boldsymbol{\eta} = \left[(\mathbf{p}^n)^T, \boldsymbol{\Theta}^T \right]^T = [n, e, d, \phi, \theta, \psi]^T. \quad (1)$$

The *body-fixed* reference frame $\{b\} = (x_b, y_b, z_b)$ with origin o_b is a moving reference frame that is fixed to the vessel. The x_b-axis is positive towards the bow, the y_b-axis is positive towards starboard, and the z_b-axis is positive downwards. The origin o_b is located midships at the waterline, with the z_b-axis passing through the center of gravity of the vessel. The $\{b\}$-frame linear velocities $\mathbf{v}_o^b = [u, v, w]^T$ and angular velocities $\boldsymbol{\omega}^b = [p, q, r,]^T$ are

$$\boldsymbol{\nu} = \left[\left(\mathbf{v}_o^b\right)^T, \left(\boldsymbol{\omega}^b\right)^T \right]^T = [u, v, w, p, q, r]^T. \quad (2)$$

The *seakeeping* inertial reference frame $\{s\} = (x_s, y_s, z_s)$ is a reference frame which is fixed to the equilibrium state of the vessel. This means that it moves along the path of the vessel with the mean forward speed U of the vessel, with respect to the $\{n\}$-frame. In absence of wave excitation, the $\{s\}$-frame origin, o_s, coincides with the $\{b\}$-frame origin, o_b. The x_b-axis is positive towards the bow, the y_b-axis is positive towards starboard, and the z_b-axis is positive downwards. The $\{s\}$-frame perturbation vector is

$$\boldsymbol{\xi} = [\xi_1, \xi_2, \xi_3, \xi_4, \xi_5, \xi_6]^T. \quad (3)$$

The rigorous mathematical transformations between these reference frames are given in Fossen (2011).

2.2 Equations of motion

The time-domain seakeeping equations of motion in $\{s\}$ for a vessel with no forward speed are given as (Fossen, 2011)

$$\begin{aligned} &[\mathbf{M}_{RB} + \mathbf{A}(\infty)]\, \ddot{\boldsymbol{\xi}} + \mathbf{B}_{total}(\infty)\dot{\boldsymbol{\xi}} \\ &\quad + \int_0^t \mathbf{K}(t-\tau)\dot{\boldsymbol{\xi}}(\tau)d\tau + \mathbf{G}\boldsymbol{\xi} = \boldsymbol{\tau}_{exc}, \end{aligned} \quad (4)$$

where the matrix of retardation functions, $\mathbf{K}(t)$, is given as

$$\mathbf{K}(t) = \frac{2}{\pi}\int_0^\infty [\mathbf{B}_{total}(\omega) - \mathbf{B}_{total}(\infty)]\cos(\omega t)d\omega. \quad (5)$$

$\mathbf{M}_{RB}$ is the rigid body mass matrix, $\mathbf{A}(\infty)$ is the added mass matrix for infinite frequency, $\mathbf{B}_{total}(\infty)$ is the damping matrix for infinite frequency including both potential and viscous damping, $\mathbf{G}$ is the restoring force matrix, and $\boldsymbol{\tau}_{exc}$ is a vector containing excitation forces.

VeSim needs all external forces to be given in the $\{b\}$-frame. Therefore, the equations of motion, Eq. 4, should be transformed from the $\{s\}$-frame to the $\{b\}$-frame. When transforming the equations of motion to the rotating $\{b\}$-frame, Coriolis forces between $\{s\}$ and $\{b\}$ appear when we have a forward speed. The equations of motion in $\{b\}$ then become (Fossen, 2011)

$$\begin{aligned} &[\mathbf{M}_{RB} + \mathbf{A}_U(\infty, U)]\, \dot{\boldsymbol{\nu}} + \mathbf{C}^*_{RB}\boldsymbol{\nu} \\ &\quad + \mathbf{B}_{total,U}(\infty, U)\boldsymbol{\nu}_r \\ &\quad + \int_0^t \mathbf{K}_U(t-\tau, U)[\boldsymbol{\nu}(\tau) - U\mathbf{e}_1]d\tau \\ &\quad + \mathbf{G}\boldsymbol{\eta} = \boldsymbol{\tau}_{exc}, \end{aligned} \quad (6)$$

where $\mathbf{C}^*_{RB}$ are Coriolis forces due to the rotation of $\{b\}$ about $\{s\}$, as derived in a linearized version in Fossen (2011), and $\mathbf{e}_1$ is the unit vector in x_b-direction. Subscript U denotes speed-dependence. $\boldsymbol{\nu}_r$ includes ocean currents. The speed-dependent added mass and damping coefficients are calculated using the strip theory by Salvesen et al. (1970). The retardation function is now calculated using the speed-dependent damping matrices, as

$$\begin{aligned} \mathbf{K}_U(t, U) = \frac{2}{\pi}\int_0^\infty &[\mathbf{B}_{total,U}(\omega, U) \\ &- \mathbf{B}_{total,U}(\infty, U)]\cos(\omega t)d\omega. \end{aligned} \quad (7)$$

VeSim first solves Eq. 6 for the vessel accelerations in $\{b\}$. Then, the accelerations are integrated to find the vessel velocities in $\{b\}$. The vessel velocities are then transformed into the $\{n\}$-frame and integrated once again to obtain the vessel positions in $\{n\}$ (Fathi, 2012).

3 FOIL IMPLEMENTATION IN VESIM

3.1 Foil definitions

The effect of fixed horizontal foils mounted to a ship was implemented in VeSim. The user inputs were the longitudinal position of the foil relative to the aft perpendicular (AP), the vertical position of the foil relative to the baseline of the ship, the transverse position of the root and tip of the foil relative to the centerline of the ship, and the chord length of the root and tip of the foil. The foil root and tip positions were taken as the position of the quarter-chord of the root and tip. The foil was divided into 10 sections of equal width, from the root to the tip. A single foil was composed by two foils with adjacent roots. Fluid velocities and accelerations parallel and perpendicular to the foil were found at the spanwise center of each section, at the 3/4-chord location, through linear interpolation between the values at the foil root and tip. The quasi-static angles of attack for all sections were calculated from these velocities.

The forces used in the implemented dynamic stall model are normal and chordwise forces, instead of lift and drag. This is convenient since VeSim requires the forces acting on the ship to be given in the ship-fixed reference frame. Fig. 1 shows the relation between these two ways of decomposing the resultant force, R, acting on a foil.

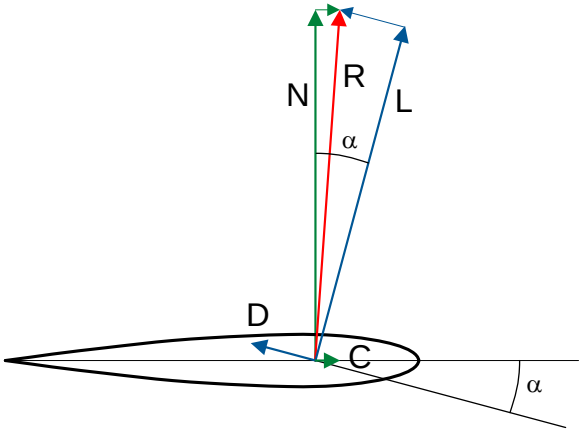

Figure 1: The relation between lift (*L*), drag (*D*), normal (*N*), and chordwise (*C*) forces and the resultant force (*R*). α is the angle of attack.

From the lift and drag, the normal and chordwise forces can be found from

$$N = L\cos\alpha + D\sin\alpha, \quad (1)$$
$$C = L\sin\alpha - D\cos\alpha, \quad (2)$$

and vice versa,

$$L = N\cos\alpha + C\sin\alpha, \quad (3)$$
$$D = N\sin\alpha - C\cos\alpha. \quad (4)$$

3.2 Dynamic stall model

3.2.1 Attached flow

The Beddoes-Leishman (B-L) dynamic stall model (Leishman & Beddoes, 1989) was implemented with some minor simplifications, as described here. If there is a small change in angle of attack for fully attached flow, it will take some time before the separation point is reestablished at the trailing edge. The circulatory normal force coefficient due to an accumulating series of step inputs in angle of attack can be expressed as

$$C^C_{N,n} = C_{N_\alpha}(\alpha_n - \alpha_0 - X_n - Y_n) \quad (5)$$
$$= C_{N_\alpha}(\alpha_{E,n} - \alpha_0), \quad (6)$$

where C_{N_α} is the normal force coefficient curve slope at the zero-lift angle of attack, α is the geometric angle of attack, α_0 is the zero-lift angle of attack, and α_E is called the effective angle of attack. Subscript n denotes time step n. X and Y are deficiency functions given by

$$X_n = X_{n-1}e^{-b_1\Delta S} + A_1(\alpha_n - \alpha_{n-1})e^{-b_1\frac{\Delta S}{2}}, \quad (7)$$

$$Y_n = Y_{n-1}e^{-b_2\Delta S} + A_2(\alpha_n - \alpha_{n-1})e^{-b_2\frac{\Delta S}{2}}, \quad (8)$$

where A_1, A_2, b_1 and b_2 are profile dependent variables describing the time delay, and ΔS is the distance traveled by the foil in semi-chords during a time interval $\Delta t = t_n - t_{n-1}$. Here, $A_1 = 0.165$, $A_2 = 0.335$, $b_1 = 0.0455$ and $b_2 = 0.3$.

The noncirculatory normal force coefficient, also known as the added mass force coefficient, was found for each section from the fluid acceleration perpendicular to the section, according to the formula for the added mass force on a heaving flat plate (Newman, 1977),

$$C^I_{N,n} = \frac{\frac{\rho\pi c^2}{4}\dot{w}_n}{\frac{1}{2}\rho V_n^2 c} = \frac{\pi c\dot{w}_n}{2V_n^2}, \quad (9)$$

where ρ is the mass density of sea water, $\dot{w}$ is the fluid acceleration perpendicular to the section at the midchord, c is the chord length, and V is the inflow speed to the foil. Finding the noncirculatory normal force coefficient without the use of a deficiency function, as done here and in Hansen et al. (2004), is a simplification relative to the original B-L model, which uses a deficiency function to account for time-history effects.

The total normal force coefficient during attached flow conditions, C^p_N, is found by summing the circulatory and noncirculatory coefficients:

$$C^p_{N,n} = C^I_{N,n} + C^C_{N,n}. \quad (10)$$

3.2.2 Trailing edge separation

The basic assumption of the B-L model is that the normal force coefficient, C_N, during separated flow can be found from

$$C_N = C_{N_\alpha}\left(\frac{1+\sqrt{f}}{2}\right)^2(\alpha - \alpha_0), \quad (11)$$

which is an approximation to the normal force coefficient on a flat plate in a potential Kirchhoff flow (Thwaites, 1960). The attachment degree, f, is defined as the distance along the chord from the leading edge to the separation point, divided by the chord length. For fully attached flow, $f = 1$, and $C_N = C_{N_\alpha}(\alpha - \alpha_0)$.

f is found from Eq. 11 by replacing the predicted C_N with the original static normal force coefficient, C^{orig}_N, so that

$$f = \left(2\sqrt{\frac{C^{orig}_N(\alpha_n)}{C_{N_\alpha}(\alpha_n - \alpha_0)}} - 1\right)^2. \quad (12)$$

For unsteady conditions, there is a lag in the leading edge pressure response with respect to C^p_N, expressed as

$$C'_{N,n} = C^p_{N,n} - D_{p,n}, \quad (13)$$

where D_p is the attached flow deficiency function

$$D_{p,n} = D_{p,n-1}e^{-\frac{\Delta S}{T_p}} + (C^p_{N,n} - C^p_{N,n-1})e^{-\frac{\Delta S}{2T_p}}. \quad (14)$$

T_p is a time constant for the pressure delay of attached flow, chosen here to be 1.5 semi-chords. An equivalent angle of attack, α_f, is defined as

$$\alpha_{f,n} = \frac{C'_{N,n}}{C_{N_\alpha}} + \alpha_0, \quad (15)$$

and the corresponding attachment degree is calculated using Eq. 12 as

$$f'_n = \left(2\sqrt{\frac{C_N^{orig}(\alpha_{f,n})}{C_{N_\alpha}(\alpha_{f,n} - \alpha_0)}} - 1 \right)^2 . \quad (16)$$

In addition to the pressure lag, there will be a viscous lag due to the unsteady boundary layer response, represented by a first-order lag to the value of f' as

$$f''_n = f'_n - D_{f,n}, \quad (17)$$

where D_f is the attachment degree deficiency function

$$D_{f,n} = D_{f,n-1} e^{-\frac{\Delta S}{T_f}} + (f'_n - f'_{n-1}) e^{-\frac{\Delta S}{2T_f}} . \quad (18)$$

T_f is a time constant for the lag in the boundary layer, chosen here to be 5 semi-chords.

The normal force coefficient incorporating both the pressure and the viscous lag is computed using Eq. 11 as

$$C^f_{N,n} = C_{N_\alpha} \left(\frac{1 + \sqrt{f''_n}}{2} \right)^2 (\alpha_{E,n} - \alpha_0). \quad (19)$$

3.2.3 Leading edge separation

As the absolute value of the angle of attack increases from zero, a vortex builds up at the leading edge. The forces and moments can be represented by ignoring the developing vortex until it detaches and is transported downstream (Leishman & Beddoes, 1989). The leading edge vortex is assumed to detach, for a symmetric foil, when the absolute value of the angle of attack is larger than a certain value, denoted α_v, and to travel downstream at a speed of $1/3$ times the inflow speed to the foil, V (Larsen et al., 2007). α_v can be found from the static moment coefficient curve, where there is a break in the pitching moment (Pereira, 2010). A nondimensional variable τ is introduced to keep track of the position of the traveling vortex. When $\tau = 0$, the vortex is at leading edge, and when $\tau = 1$, the vortex has reached the trailing edge. $\tau = 0$ unless $|\alpha| > \alpha_v$, when τ increases as

$$\tau_n = \tau_{n-1} + \frac{V_n}{3c} \Delta t. \quad (20)$$

The increment in the vortex induced normal force coefficient due to a vortex at the leading edge, C_V, is determined by the difference between the instantaneous linearized value of the unsteady circulatory normal force coefficient and the corresponding unsteady nonlinear normal force coefficient as given by the Kirchhoff approximation,

$$C_{V,n} = C^C_{N,n} - C^f_{N,n}. \quad (21)$$

The total accumulated vortex induced normal force coefficient, C^V_N, is allowed to decay exponentially with time, but may also be updated by a new increment:

$$C^V_{N,n} = C^V_{N,n-1} e^{-\frac{\Delta S}{T_v}} + (C_{V,n} - C_{V,n-1})\, e^{-\frac{\Delta S}{2T_v}}, \quad (22)$$

if the vortex is growing in strength and located on the foil surface. T_v is a time constant for vortex delay and was chosen here to be 6 semi-chords. If the vortex is no longer on the foil surface and thus decreasing in strength, or it is on the foil surface but decreasing in strength without detaching, Eq. 22 reduces to

$$C^V_{N,n} = C^V_{N,n-1} e^{-\frac{\Delta S}{T_v}} . \quad (23)$$

Finally, the total normal force coefficient becomes

$$C_{N,n} = C^f_{N,n} + C^V_{N,n}. \quad (24)$$

3.2.4 Chordwise force

The chordwise force coefficient is calculated as

$$C_{C,n} = \eta C_{N_\alpha}(\alpha_{E,n} - \alpha_0)\alpha_{E,n}\sqrt{f''_n} - C_{D0}, \quad (25)$$

where η is called the recovery factor, which accounts for the fact that the foil does not realize 100 percent of the chordwise force attained in potential flow. $\eta = 0.95$ was used here (Leishman & Beddoes, 1989). The first term on the right hand side of Eq. 25 includes the effects of both pressure and viscous lag, but it represents only the pressure contribution to the normal force. Viscous effects are included through the term C_{D0}, which is the viscous drag coefficient at zero lift.

3.3 Resulting foil forces

The normal force, $N(y_0)$, and the chordwise force, $C(y_0)$, of each section of the foil were calculated as

$$N(y_0)_n = C_{N,n}(y_0) \frac{1}{2} \rho V_n(y_0)^2 c(y_0) ds \quad (26)$$

and

$$C(y_0)_n = C_{C,n}(y_0) \frac{1}{2} \rho V_n(y_0)^2 c(y_0) ds, \quad (27)$$

where y_0 is the spanwise center of the foil section where the two-dimensional forces are calculated, and ds is the section width. $C_N^{orig}(\alpha_f)$ was found from section lift and drag coefficients given in Sheldahl & Klimas (1981) (actually taken from Lazauskas (2004), who corrected anomalies in the original data), with α_f and Reynolds number, Re, at the spanwise center of each strip, y_0, as inputs. C_{N_α} and C_{D0} were found similarly, but with the angle of attack input being the zero-lift angle of attack.

The total normal and chordwise forces for the foil were found by summing the sectional forces. The foil forces were then added to the excitation forces, $\boldsymbol{\tau}_{exc}$, on the right side of Eq. 6.

4 SIMULATIONS

4.1 Regular head sea waves

A 90 m long offshore vessel employing a fixed foil of 29 m span in the bow was simulated using VeSim. This is the same ship and foil that was tested in the model tests described in Sec. 5. The waves used in the simulations were the same as in the model tests, namely head sea waves, with wave heights and periods given in Table 3. Results are presented and compared with model tests in Fig. 5, and

discussed in Sec. 6. The drag of the struts was found from model tests, Froude-scaled to full scale, and included in the simulated resistance and foil thrust.

4.2 Effect of wave direction

For regular waves with height 3 m and period 8.5 s, the wave direction relative to the heading of the ship was varied from 0 to 180 degrees in increments of 15 degrees. The foil was of the same dimensions and located at the same position as described in Sec. 5. A polar diagram of the propulsive thrust as a function of wave direction is shown in Fig. 2. As shown in Fig. 2, the most beneficial wave directions ranged from 0 to $\pm$ 75 degrees. Little thrust was produced in following seas, but in that case, the ship was helped forward by the wave drift force.

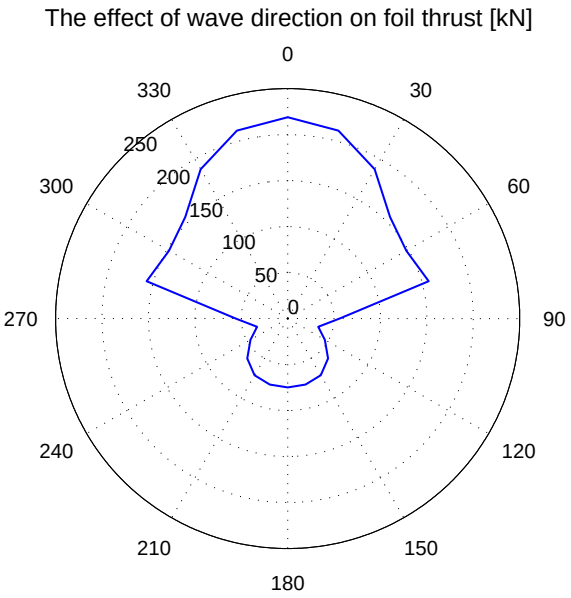

Figure 2: The effect of wave direction on foil thrust from simulations of a ship with a fixed foil in the bow, sailing at a speed of 12 knots in regular waves with height 3 m and period 8.5 s.

4.3 Effect of foil position

For regular head sea waves with height 2 m and lengths 0.6, 1.2 and 2.0 times the ship length, the longitudinal position of the foil was varied. The vertical position was the same as described in Sec. 5. Naito et al. (1986) plotted the nondimensional thrust as a function of foil position for the same wavelength/ship length-ratios, and found that, for a wavelength/ship length-ratio of 1.2, maximum thrust was produced when the foil was located slightly in front of the bow. A similar plot based on our simulations is shown in Fig. 3, but we have chosen to nondimensionalize the thrust, T, by dividing it by $\rho g \zeta_a^2 L_{PP}$, where g is the acceleration of gravity, ζ_a is the wave amplitude, and L_{PP} is the length between perpendiculars. Fig. 3 bears striking resemblance to Fig. 9 in Naito et al. (1986), which is reproduced as Fig. 13 in Naito & Isshiki (2005). The ideal position of the foil for a wavelength of 1.2 times the ship length, corresponding to a wave period of 8.32 s in our case, was slightly in front of the bow, or quite far aft of the stern, where it is difficult to place a foil in reality.

5 MODEL TESTS

Model tests of an offshore vessel (Rolls-Royce design UT 751 E) with a fixed foil in the bow were performed in the MARINTEK towing tank. The model test setup is shown in Fig. 4. The ship model was towed from wires attached to an aluminum beam, which was mounted perpendicular to the hull, as shown in Fig. 4. This enabled the ship to move freely in heave and pitch, while constrained in yaw. The surge motion of the model was limited by springs connecting the towing wires to the seakeeping carriage. The main particulars of the ship and foil in model and full scale are given in Tables 1 and 2. The foil was located 8.761 m below the baseline of the ship, with the quarter chord located 79.005 m ahead of the AP, in full scale.

Main particular	Ship	Model
Length on waterline (L_{WL})	90.144 m	5.634 m
Length between perpendiculars (L_{PP})	80.800 m	5.050 m
Beam	21.000 m	1.313 m
Draft	4.300 m	0.269 m
Wetted surface area	1864.654 m^2	7.284 m^2
Displaced volume	4917.270 m^3	1.201 m^3

Table 1: Main particulars of the ship for the waterline used in the model tests.

Main particular	Ship	Model
Profile	NACA 0015	NACA 0015
Span	28.96 m	1.81 m
Maximum chord	3 m	0.1875 m
Projected area	81.8721 m^2	0.319813 m^2
Aspect ratio	10.24	10.24

Table 2: Main particulars of the foil.

The model was supposed to be exposed to head sea regular waves with full-scale wave height 3 m, and full-scale wave periods ranging from 6.5 to 11.5 s. The actual waves generated were, however, somewhat different. The actual wave heights and wave periods used in the model tests, found from wave height measurements, are given in Table 3. In order to compare model tests and simulations, the same wave conditions were used in the simulations. The ship model was also tested in the same conditions without the foil, in order to study the effect of the foil.

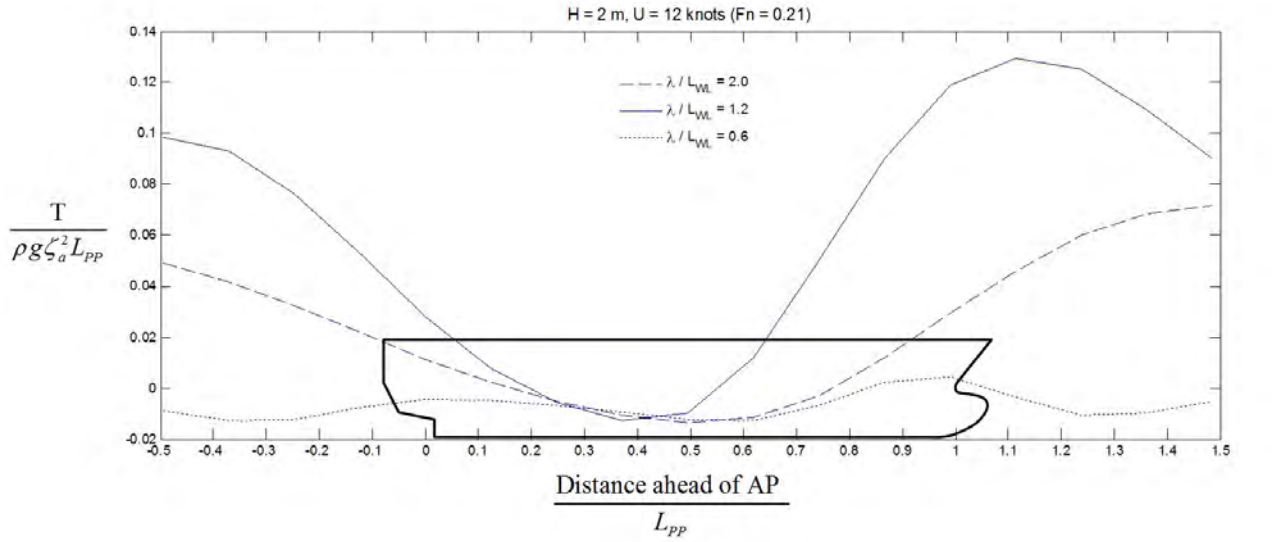

Figure 3: Nondimensional thrust as a function of foil position, for regular head sea waves with height 2 m.

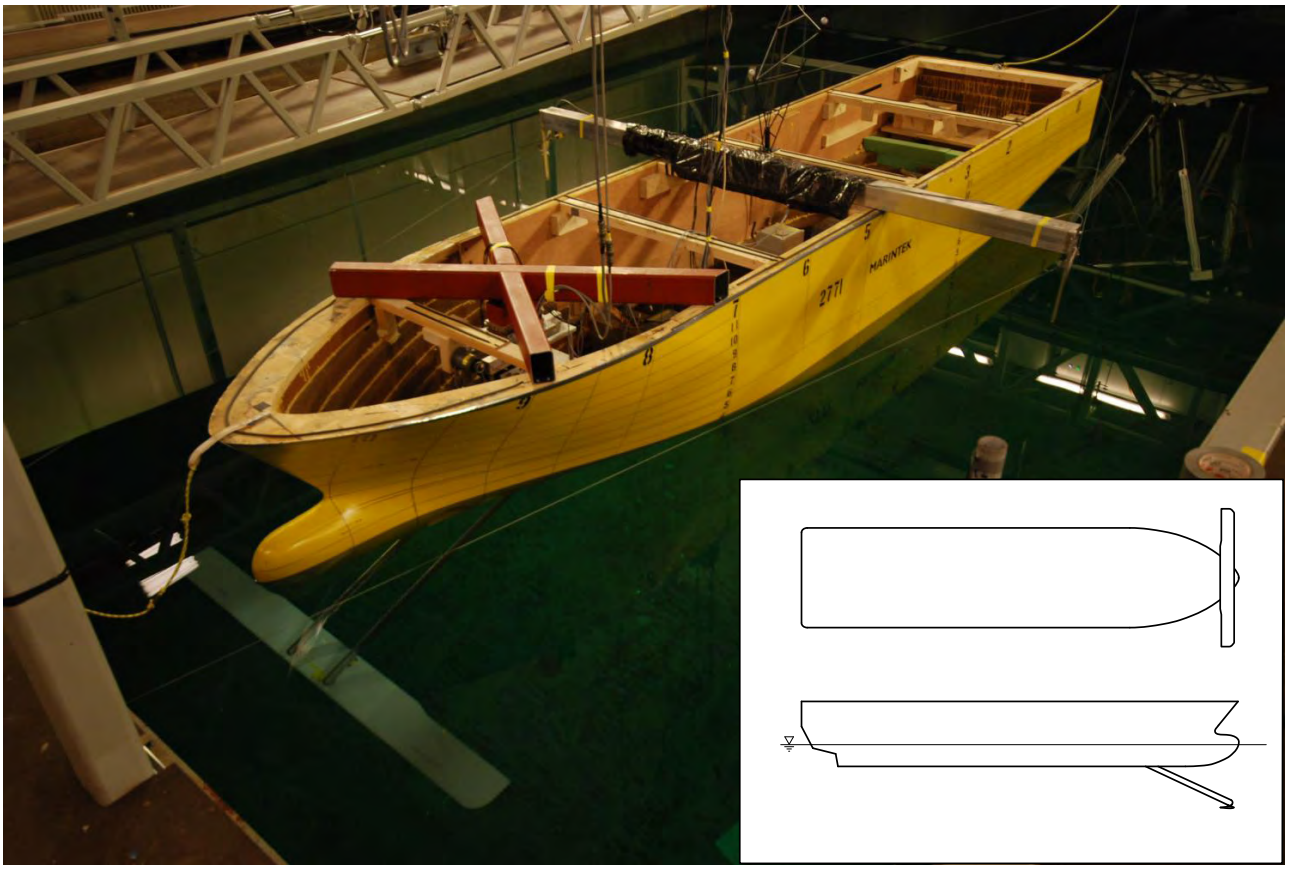

Figure 4: Model test setup.

Without foil		With foil	
T [s]	H [m]	T [s]	H [m]
11.107	3.734	11.107	3.640
10.668	3.666	10.305	3.652
9.630	3.473	9.630	3.568
8.555	3.739	8.555	3.712
7.561	4.417	7.561	4.329
6.563	3.584	6.563	3.664

Table 3: Wave periods (T) and heights (H) used in the model tests and simulations.

6 DISCUSSION OF RESULTS

For the ship without foil, there was good agreement between the experimental and simulated RAOs in heave and pitch for wave periods shorter than 8.6 s. For higher wave periods, the simulated values were significantly different from the experimental values, as shown in Fig. 5. A verification study with the frequency-domain strip theory program VERES was inconclusive regarding the correct heave RAO for these wave periods, but supported the pitch RAO found with VeSim.

The foil thrust was dependent on Re, as shown in Fig. 5. Froude-scaling the model test resistance to full scale implies that the full-scale Froude number, Fr, is correct, but not the full-scale Re. Using model-scale Re when simulating full-scale foil thrust should therefore give better agreement with the Froude-scaled thrust from the model tests, as in Fig. 5. The reason for this is that the foil will stall for a lower angle of attack with model-scale Re than with full-scale Re, as shown in Fig. 6a. In addition, the drag coefficient is higher in model scale than in full scale, significantly so for angles of attack between 15 and 20 degrees, as shown in Fig. 6b. Hence, if the angle of attack was sufficiently high, the thrust using model-scale Re was lower than the thrust using full-scale Re.

The simulated full-scale thrust with model-scale Re was substantially higher than the Froude-scaled full-scale thrust found from the model tests. This is believed to be due to elasticity in the wire that held the foil fixed in the model tests. Model tests with the foil alone showed that the foil could quite easily be turned a few degrees despite the wire, which was supposed to hold it in place. In order to model this effect in the simulations, the elastic wire was represented by a fictional spring located at the midchord. The stiffness of this spring was found by comparing a test where the foil was towed alone, i.e., without the ship, with simulated forces. The simulated thrust with the spring at the midchord was in good agreement with the thrust from the model tests, as shown in Fig. 5. This supports that the dynamic stall model was working well, and that the resistance from the model tests would most likely have corresponded better with the simulated resistance had the foil been completely fixed. Three-dimensional effects on lift and drag were not accounted for in the strip theory for the foil forces and could also cause deviation from the model test results.

From the discussion above, it is no surprise that the simulated ship motions for the ship with foil were not in very good agreement with the model test results, as shown in Fig. 5. The general trends of the graphs with respect to wave period and foil effects, however, seem to be quite well captured.

The fixed foil in the bow reduced the resistance by 60% in regular head sea waves with height 3.7 m and period 8.6 s, according to the model tests. For the same wave and ship speed, the vessel's heave and pitch motions were reduced by 42% and 45%, respectively. The simulated resistance for the ship without foil was in good agreement with the ship resistance from the model tests. The simulated ship resistance for the ship with foil, however, was overpredicted for the two shortest wave periods, and underpredicted for the four longest wave periods. The underprediction in resistance is believed to be caused by the overpredicted foil thrust, due to the model test foil not being entirely fixed.

7 CONCLUSIONS AND FUTURE WORK

As observed during the model tests, a fixed foil in the bow reduced the heave and pitch motions significantly in regular head sea waves because the net force produced by the foil generally opposed the motion of the ship. This motion reduction, in addition to the thrust being created by the foil, resulted in a dramatic resistance reduction in the waves that produced the largest ship motions. The effect of the foil on the ship was implemented in the MARINTEK Vessel Simulator (VeSim). The simulated heave and pitch motions did not match the experimentally found heave and pitch motions with satisfying accuracy for all wave periods, but the general wave period and foil effects were reasonably well captured. The foil thrust from the model tests was shown to be lower than the simulated foil thrust mainly due to elasticity in the wire that held the foil fixed. In other words, had the foil in the experiments been completely fixed, the simulated and experimentally found results would have been in better agreement.

The foil produced maximum thrust when located slightly in front of the bow of the ship for wavelengths equal to or somewhat longer than the ship length. The most beneficial wave directions with respect to the foil thrust were 0 (head sea) to $\pm$ 75 degrees.

The theoretical foil model appeared to work well for fixed foils, and can be extended to foils that move relative to the ship. The first future development is the extension of the theoretical foil model to account for actively controlled pitching foils, in order to maximize the thrust from the foils in waves.

ACKNOWLEDGEMENTS

The authors would like to thank Dariusz Fathi at MARINTEK for invaluable help with the VeSim software. Anders Jahre's Fund for the Promotion of Science is acknowledged for financing the foil and complementary equipment. Rolls-Royce Marine is acknowledged for financing the model tests and allowing the modification of their ship model. In addition, the authors are grateful to Torgeir Wahl at NTNU and Morten Korsvold and Alexander Sandnes

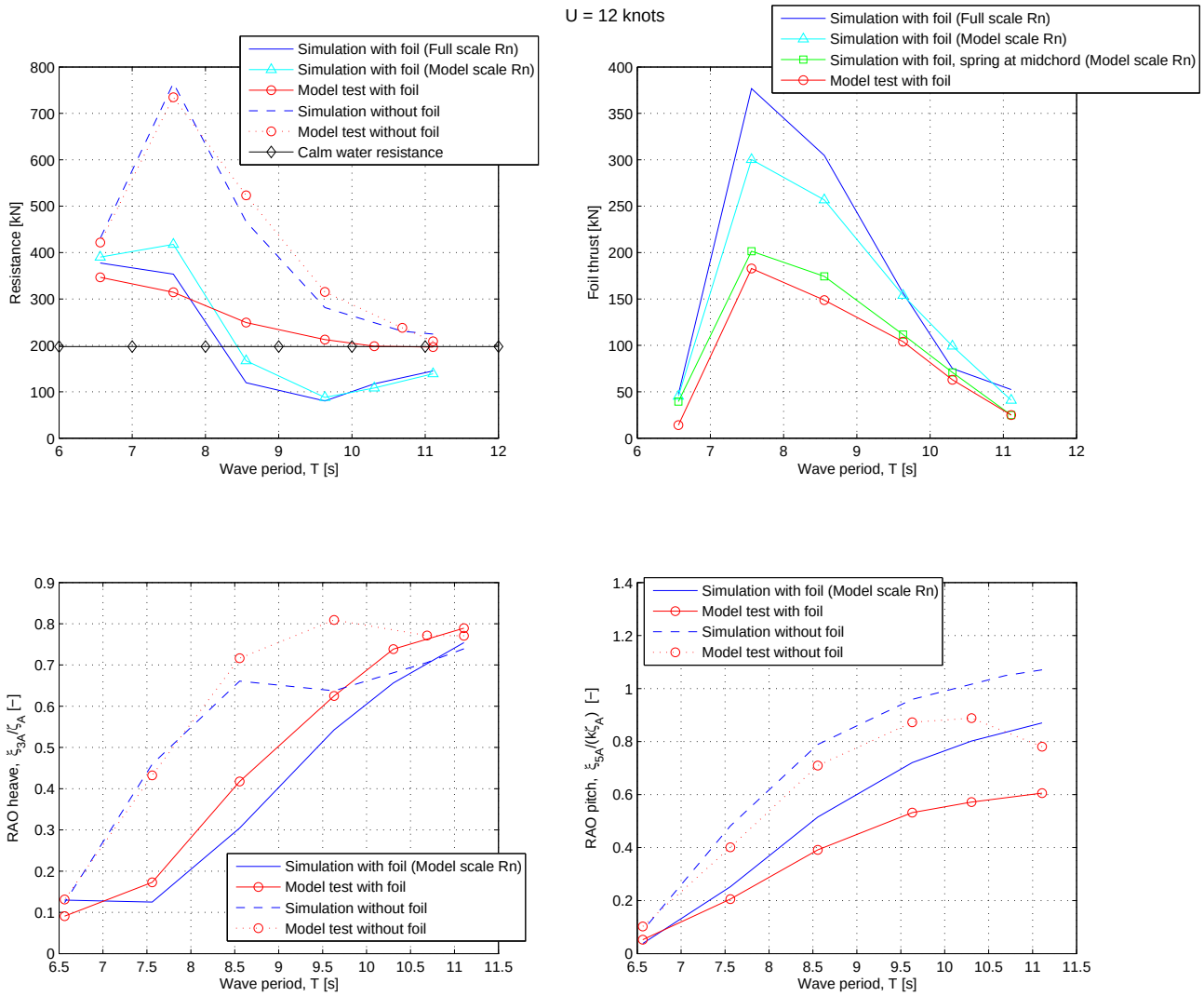

Figure 5: Simulation vs. Froude-scaled model test results for the full-scale ship with a fixed bow-foil, sailing at a speed of 12 knots in regular head sea waves. Wave heights used are given in Table 3.

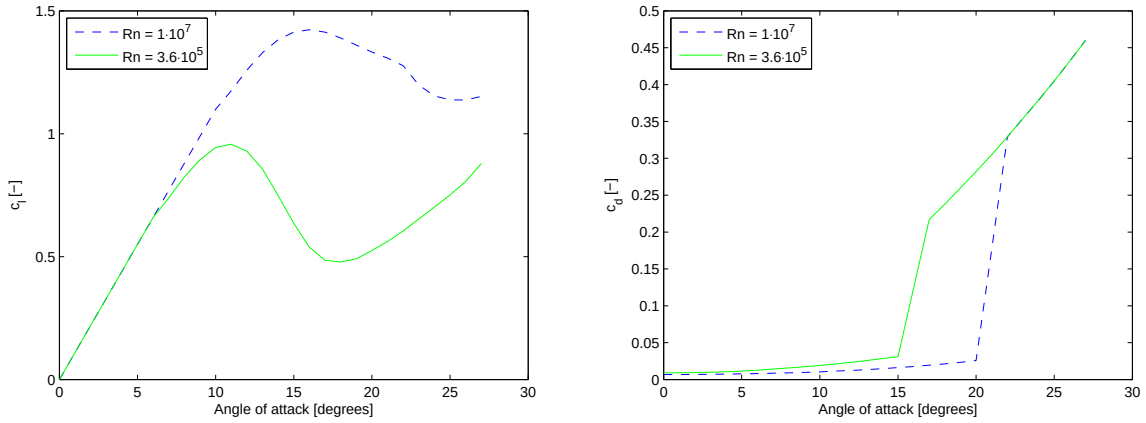

(a) Lift coefficient curves

(b) Drag coefficient curves

Figure 6: Static section lift and drag coefficient curves from Sheldahl & Klimas (1981) for Re=360,000 (close to model-scale Reynolds number) and Re=10,000,000 (half of full-scale Re, but the highest Re Sheldahl & Klimas (1981) provide c_l and c_d for).

at MARINTEK for their support with the experiments described in this paper.

REFERENCES

Ashburton Guardian, 1897. 'A Boat with Fins'. Volume XVIII, Issue 4281, 30 August 1897.

Bose, N. & Lien, J., 1990. 'Energy Absorption from Ocean Waves: A Free Ride for Cetaceans'. Proc. R. Soc. Lond., **B 240**. pp. 591–605.

Burnett, R. F., 1979. 'Wave Energy for Propelling Craft - Nothing New'. The Naval Architect. Nov. 1979, p. 239.

Fathi, D., 2012. MARINTEK Vessel Simulator (VeSim), Vessel Model. MARINTEK. Rev. 4.

Fossen, T. I., 2011. Handbook of Marine Craft Hydrodynamics and Motion Control. 1st ed. John Wiley & Sons, Ltd.

Hansen, M. H., Gaunaa, M. & Madsen, H. A., 2004. 'A Beddoes-Leishman Type Dynamic Stall Model in State-Space and Indicial Formulations'. Tech. Rep. Risø-R-1354(EN), Risø National Laboratory, Roskilde, Denmark.

Hoff, J. R., 2007. 'Unified Formulation for Seakeeping and Maneuvering'. Tech. Rep. 540054.00.03, MARINTEK.

Jakobsen, E., 1981. 'The Foilpropeller, Wave Power for Propulsion'. Second International Symposium on Wave & Tidal Energy. BHRA Fluid Engineering, pp. 363–369.

Larsen, J. W., Nielsen, S. R. K. & Krenk, S., 2007. 'Dynamic Stall Model for Wind Turbine Airfoils'. Journal of Fluid and Structures, **23**, pp. 959–982.

Lazauskas, L., 2004. 'Airfoil Data'. http://www.cyberiad.net/foildata.htm. Retrieved August 15, 2012.

Leishman, J. G. & Beddoes, T. S., 1989. 'A Semi-Empirical Model for Dynamic Stall'. Journal of the American Helicopter Society, **34**(3), pp. 3–17.

Naito, S. & Isshiki, H., 2005. 'Effect of Bow Wings on Ship Propulsion and Motions'. Applied Mechanics Reviews, **58**(4), pp. 253–268.

Naito, S., Isshiki, H. & Fujimoto, K., 1986. 'Thrust Generation of a Fin Attached to a Ship in Waves'. Journal of the Kansai Society of Naval Architects, Japan, **202**, pp. 23–28. In Japanese.

Newman, J. N., 1977. Marine Hydrodynamics. The MIT Press.

NIMA, 1997. 'Department of Defense World Geodetic System 1984'. Tech. Rep. TR8350.2, NIMA.

Pereira, R. B. d. S., 2010. 'Validating the Beddoes-Leishman Dynamic Stall Model in the Horizontal Axis Wind Turbine Environment'. M.Sc. Thesis, Instituto Superior Técnico, Lisbon.

Politis, G. & Politis, K., 2012. 'Biomimetic Propulsion under Random Heaving Conditions, Using Active Pitch Control'. Journal of Fluid and Structures.

Salvesen, N., Tuck, E. O. & Faltinsen, O., 1970. 'Ship Motions and Sea Loads'. Transactions SNAME, **78**, pp. 250–287.

Sheldahl, R. E. & Klimas, P. C., 1981. 'Aerodynamic Characteristics of Seven Symmetrical Airfoil Sections Through 180-Degree Angle of Attack for Use in Aerodynamic Analysis of Vertical Axis Wind Turbines'. Tech. Rep. SAND80-2114, Sandia National Laboratories.

The New York Times, 1898. 'A Self-Propelling Boat'. December 18, 1898.

Thwaites, B., 1960. Incompressible Aerodynamics. Clarendon Press, Oxford.

Vrooman, D., 1858. 'Vibrating Propeller'. US Patent 22,097. Patented Nov. 15, 1858.